Catastrophes of Elastic Column Structures

AUTHOR(S):

NIWA, Yoshiji; WATANABE, Eiichi; ISAMI, Hidenori

Catastrophes of Elastic Column Structures

By

Yoshiji NIWA*, Eiichi WATANABE** and Hidenori ISAMI***

(Received December 17, 1982)

Abstract

The elasto-static instability phenomena of structures can be typically classified by the catastrophe theory in the local form near a certain singular point of their total potential energy. Then, the imperfection sensitivity of the structures can be evaluated in terms of the bifurcation set, mapping the singular points of the equilibrium space to the control space. In ordinary structural problems, this consists of a simple loading parameter and some imperfection parameters.

In this paper, several simplified column models are studied by the catastrophe theory. They include both continuous and discrete models exhibiting stable symmetric, unstable symmetric, asymmetric and their compound buckling. From a comparison of the results of the two-degree-of-freedom systems, namely the continuous systems and the finite element discrete systems, the following conclusions are drawn:

(i) The discrete analysis can be shown to realize the instability phenomena, predicted by the continuous analysis. The results of the discrete analysis are shown to converge to those of the continuous analysis generally, as the number of discrete finite elements increases.

(ii) The imperfection sensitivity of the structures can be evaluated qualitatively and quantitatively by means of the bifurcation set in the control space through the catastrophe theory.

(iii) For a legitimate evaluation of the "cusp and dual cusp catastrophe", the 4th order non-linear terms must be earnestly considered in expressions for both the strain energy and the external work. Then, the stable symmetric buckling model is shown to indicate a typical cusp catastrophe.

(iv) The unstable symmetric buckling model can be shown to indicate a typical dual cusp catastrophe for a relatively small stiffness of the elastic foundation, the cusp catastrophe for a relatively large stiffness and the compound double cusp catastrophe at a certain critical stiffness value.

(v) The asymmetric buckling model can be shown to indicate the typical fold catastrophe for a relatively small stiffness of the inclined elasic foundation, the dual cusp catastrophe for a relatively large stiffness and the compound hyperbolic umbilic catastrophe at a certain critical stiffness value.

1. Introduction

Studies on the stability of equlibrium states of continous systems were developed

*Dr. Eng., Professor, **Ph. D., Associate Professor, and ***M.S., Research Associate, Kohchi Technical College, Kohchi (formerly Graduate Student, Kyoto University)

by Euler and Lagrange. Poincare discussed the general bifurcation theory in terms of the topology of differential equations. Liapunov defined mathematically the stability from the viewpoint of the convergence of arbitrary perturbations. Also, Koiter unified the non-linear elastic bifurcation theory of continuous systems[1] and, together with Budiansky and Huchinson, investigated the general elastic stability theory. This included the post-buckling behavior and the imperfection sensitivity of structures in the form of a Taylor expansion about a singular point of the total potential energy. Furthermore, applications of the generalized coordinates to this non-linear instability phenomenon had been accomplished by Thompson.[2]

On the other hand, independently from those people just mentioned, topologist R. Thom treated such bifurcation phenemena as singular points of mappings. He called this the "Catastrophe Theory", and published "Structural Stability and Morphogeneses".[3] In the catastrophe theory, the discontinuous phenomenon can be caused even by certain continuous changes of the relevant parameters, and the discussion is focussed on the singularity of the mappings. Zeeman clarified the feasibility of the applications of this catastrophe theory to Euler's bifurcation problem.[4]

Thompson and Hunt established the relationship between the non-linear elastic bifurcation buckling theory and the topological catastrophe theory, that is, those between the symmetric buckling, asymmetric buckling and limit points in the former theory and the so-called Thom's seven elementary catastrophes in the latter.[5,6,7]

The present paper presents a comparative study on the continuous analyses and discrete analyses on column models in relation to the models by Niwa et al.[8] The first stable symmetric buckling model corresponds to an elastica model, normal simple struts and rings, struts on an elastic foundation and normal thin plates subjected to in-plane loading. The stability of such models has been analyzed by Thompson in terms of the differential equation, continuous method and finite element method.[9] The second unstable symmetric buckling model corresponds to a laterally loaded shallow arch, a column on an elastic foundation, a pony truss and a cylindrical or elliptic shell subjected to an external pressure and an axial load. Furthermore, the third asymmetric buckling model corresponds to a rigid frame in the well-known Roorda experiments,[10] and in Britvec's analysis, to a complete spherical or oblate spheroidal shell under external pressure.

All the proposed models are assumed to be elastic conservative systems. Therefore, the necessary and sufficient condition of the equilibrium of the systems is the total potential energy being stationary, whereas the condition of the stability of the equilibrium systems is the second variation of the total potential energy being positive

definite.† Furthermore, these column models are assumed to be inextensible along the neutral axis. The load is assumed to act conservatively in the axial direction, being controlled by a single loading parameter. Thus, the total potential energy of a column structure can be expressed in terms of a single loading parameter, the lateral deflections and the associated prescribed initial deflections. The initial deflections are assumed in the same modes as the considered buckling modes. The other imperfection parameters such as load eccentricities and residual stresses are not considered herein.

Thus, several interesting comparisons can be made among those three catastrophe analyses: the two-degree-of-freedom analysis, the continuous analysis and the discrete analysis. The applicability and the feasibility of the proposed method are discussed in a later section.

2. Catastrophe Analysis

The load-carrying capacity of structures is generally adversely affected by imperfections such as initial deformations, eccentricities and residual stresses. This is what is called the "imperfection sensitivity of structures".

It is a general practice to solve the elasto-plastic and geometrically non-linear equilibrium equations to evaluate the load-carrying capacity. For this purpose, such numerical procedures as Newton-Raphson's, perturbation, incremental and homotopy continuation methods are commonly used. Consequently, the load-carrying capacity of structures can be plotted against the initial imperfections. However, these results can only be obtained in a discrete numerical form and are generally time-consuming.

In this respect, an application of the catastrophe theory may be found to be useful. The load-carrying capacity of structures can be evaluated explicitly by means of the bifurcation set of the catastrophe map. The catastrophe map, herein, is defined to be a map of singular points†† of equilibrium surface on the control space, spanned by a loading parameter and several imperfection parameters. The mapped surface is called the bifurcation set, designating the adverse effects of the initial imperfections. It can be evaluated without resorting to the solution process of the non-linear simultaneous equations.

---

† Another definition of the stability may read: The origin of the state space is stable if in some region about the origin, there exists a Liapunov function. See "Huseyin, K.: Vibrations and stability of multiple parameter systems, Mechanics of Elastic Stability, Sijthoff & Noordhoff, 1978."

†† A singular point of the imperfect systems may be treated differently from a singular point of the perfect systems, herein. Such a singular point of the perfect systems may be referred to as a critical point.

3. Continuous Analysis

(1) General remarks

In this section, a continuous analysis on stable symmetric, unstable symmetric and asymmetric buckling models will be presented. The discussions will be made as brief as possible here, and detailed descriptions may be provided in a reference by Niwa et al.[11]

Let $W(X)$ and $W_0(X)$ designate the lateral additional and initial deflection of column structures, respectively, where X refers to the coordinate taken along the deformed neutral axis of the column. Fig. 3.1 illustrates a simply supported column, referred to as the stable symmetric buckling model.

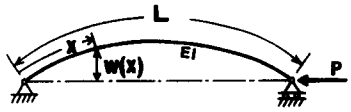

Fig. 3.1. Stable symmetric buckling model.

In the inextensible column, a curvature, κ_x, at the coordinate X can be designated as[5,9]:

$$\left.\begin{aligned}\kappa_x &= W_{,xx}\,[1-(W_{,x}+W_{0,x})^2]^{-1/2}\\ &\cong W_{,xx}+\frac{1}{2}W_{,xx}W_{,x}^2\end{aligned}\right\} \qquad \cdots\cdots(3.1)$$

where $W_{,x}=\mathrm{d}W/\mathrm{d}X$ and $W_{,xx}=\mathrm{d}^2W/\mathrm{d}X^2$.

Also, a shortening, Δ, at the right end as shown in Fig. 3.1, can be shown as:

$$\begin{aligned}\Delta &= \int_0^L [1-\{1-(W_{,x}+W_{0,x})^2\}^{1/2}]\,dx\\ &\cong \int_0^L \left(\frac{1}{2}W_{,x}^2+W_{,x}W_{0,x}+\frac{1}{8}W_{,x}^4\right)dx \qquad \cdots\cdots(3.2)\end{aligned}$$

where L is the constant total length of the column structure. In Eqs. (3.1) and (3.2), the terms of $(W_{0,x})^2$ and the higher order terms of $W_{,x}$ are assumed to be negligible.

Let us introduce the following non-dimensionalized parameters:

$$x=\frac{X}{L}, \qquad w=\frac{W}{L}, \qquad w_0=\frac{W_0}{L}, \qquad \lambda=\frac{PL^2}{EI} \qquad \cdots\cdots(3.3)$$

where EI refers to the constant flexural rigidity of the column structure, and P refers to the axial load applying at the right end.

Then, the non-dimensionalized total potential energy, V, can be obtained by

Table 3.1. Comparison of various approximations of flexural curvature and edge shortening

Approx-imation	Curvature κ_x	Shortening Δ	Remarks
1	$W_{,xx}$	$\int_0^L\left(\frac{1}{2}W_{,x}{}^2+W_{,x}W_{o,x}\right)dx$	Linear Eigen-Value Problem
2	$W_{,xx}+\frac{1}{2}W_{,xx}W_{,x}{}^2$	$\int_0^L\left(\frac{1}{2}W_{,x}{}^2+W_{,x}W_{o,x}\right)dx$	
3	$W_{,xx}$	$\int_0^L\left(\frac{1}{2}W_{,x}{}^2+W_{,x}W_{o,x}+\frac{1}{8}W_{,x}{}^4\right)dx$	
4	$W_{,xx}+\frac{1}{2}W_{,xx}W_{,x}{}^2$	$\int_0^L\left(\frac{1}{2}W_{,x}{}^2+W_{,x}W_{o,x}+\frac{1}{8}W_{,x}{}^4\right)dx$	Present Analysis, Eqs. (3.1) & (3.2)

the sum of the flexural strain energy and the external work under the axial load:

$$\left.\begin{aligned} V(w,\lambda,w_0)=&\frac{1}{2}\int_0^1(w_{,xx}^{\,2}+w_{,xx}^{\,2}w_{,x}^{\,2})\,dx\\ &-\lambda\int_0^1\left(\frac{1}{2}w_{,x}^{\,2}+w_{,x}w_{0,x}+\frac{1}{8}w_{,x}^{\,4}\right)dx\end{aligned}\right\} \quad \text{.....(3.4)}$$

where $w_{,x}=dw/dx$, $w_{0,x}=dw_0/dx$, and $w_{,xx}=d^2w/dx^2$.

Usually, however, both the second term of κ_x in Eq. (3.1) and the third term of Δ in Eq. (3.2) are not taken into account for linear bifurcation problems. Table 3.1 shows several possible combinations of approximate curvature and edge shortening. It can be shown, firstly, that the potential energy based on Approximation 1 leads only to a linear eigen value problem. Secondly, the potential energy based on Approximation 2 or 3 can be shown to fail in evaluating rigorously either the flexural strain energy or the external work. Finally, the potential energy in the last row is considered to be sufficiently rigorous, and is adopted herein in order to approximate the geometrical non-linearity.

(2) Stable Symmetric Buckling Model

Fig. 3.1 illustrates an arbitrary deformed state under a load, P. The non-dimensionalized total potential energy of the model is given by Eq. (3.4). This equation may be interpreted as the map with a lateral deflection, w, as the state variable, and load, λ, and the lateral initial deflection, w_0, being the control parameters.

The perfect column model without any initial imperfections has, in general, distinct bifurcation buckling points. The primary buckling mode is of a half sine wave.

Therefore, the modal transforms ($h_1\times h_2$) given by

$$h_1:\ w(x)=v_1\sin\pi x, \qquad \text{and } h_2:\ w_0(x)=\varepsilon_1\sin\pi x \qquad \text{.....(3.5)}$$

can be adopted to transform directly the total potential energy, V, to a new potential, A. In Eq. (3.5), v_1 and ε_1 refer to the parameters indicating the magnitude of the buckling mode and that of the imperfection of the same mode, respectively.

Upon transformation through Eq. (3.5), the Taylor expansion of the imperfect total potential energy, A, around the critical point, $(v_1, \lambda, \varepsilon_1)=(0, \pi^2, 0)$, of the perfect system, leads to[12]

$$A(v_1, \lambda, \varepsilon_1)=\frac{1}{24}A^c_{1111}v_1^4+\frac{1}{2}A^{0c}_{11}(\lambda-\lambda_c)v_1^2+A^{1c}_1 v_1\varepsilon_1 \qquad \text{.....(3.6)}$$

where

$$\left.\begin{aligned} A^c_{1111}&=\frac{3}{8}\pi^6, & A^{0c}_{11}&=-\frac{\pi^2}{2},\\ A^{1c}_1&=-\frac{\pi^4}{2}, & \lambda_c&=\pi^2. \end{aligned}\right\}$$

Since $A^c_{1111}>0$, Eq. (3.6) indicates the stable symmetric bifurcation buckling corresponding to Thom's typical cusp catastrophe. It is well-known, however, that the bifurcation set of the cusp catastrophe does not provide any realistic meaning. In such cases, the load-carrying capacity of the model should be evaluated using a certain yield criterion of the material in the elasto-plastic range. However, such elasto-plastic characteristics are beyond the scope of this paper.

(3) Unstable Symmetric Buckling Model

Let us consider a column similar to the stable symmetric model, but with an elastic foundation at the right end as shown in Fig. 3.2. Then, the non-dimensionalized total potential energy of the model is given by

$$V(w, \lambda, w_0)=\frac{1}{2}\int_0^1 (w,_{xx}^2+w,_{xx}^2 w,_x^2)\,dx$$
$$-\lambda\int_0^1\left(\frac{1}{2}w,_x^2+w,_x w_{0,x}+\frac{1}{8}w,_x^4\right)dx+\frac{k}{2}w_L^2 \qquad \text{.....(3.7)}$$

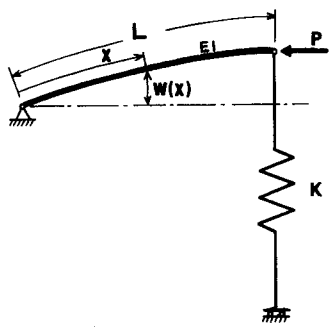

Fig. 3.2. Unstable symmetric buckling model.

where $w_L=W_L/L=W(X=L)/L$, $k=KL^3/EI$, and K refers to the spring constant of the elastic foundation.

Then, the following three typical instability phenomena can be shown to take place depending upon the magnitude of the non-dimensionalized spring rigidity, k, of the elastic foundation:

(i) when $k>\pi^2$

A distinct bifurcation with mode 2:

$$w(x)=v_2 \sin \pi x$$

may occur at the critical point $(v_2, \lambda, \varepsilon_2)=(0, \pi^2, 0)$. The mode corresponds to a half sine waveform for the column buckling configuration.

Then, the non-dimensionalized total potential energy of the imperfect model near the critical point can be expanded to the following form:

$$A(v_2, \lambda, \varepsilon_2)=\frac{1}{24}A^c_{2222}v_2^4+\frac{1}{2}A^{oc}_{22}(\lambda-\lambda_c)v_2^2+A^{2c}_2 v_2\varepsilon_2, \qquad \text{.....(3.8)}$$

where

$$\left.\begin{aligned} A^c_{2222}&=\frac{3}{8}\pi^6, & A^{oc}_{22}&=-\frac{\pi^2}{2} \\ A^{2c}_2&=-\frac{\pi^4}{2}, & \lambda_c&=\pi^2. \end{aligned}\right\}$$

Eq. (3.8) predicts the stable symmetric bifurcation buckling corresponding to Thom's cusp catastrophe. This model can behave similarly to the simply supported column without any significant effect from the elastic foundation.

(ii) when $k<\pi^2$

A distinct bifurcation with mode 1:

$$w(x)=v_1 x$$

may occur at the critical point $(v_1, \lambda, \varepsilon_1)=(0, k, 0)$. The mode corresponds to a rigid-body straight line configuration.

The non-dimensionalized total potential energy of the imperfect model near the critical point can be expanded to the following form:

$$A(v_1, \lambda, \varepsilon_1)=\frac{1}{24}A^c_{1111}v_1^4+\frac{1}{2}A^{oc}_{11}(\lambda-\lambda_c)v_1^2+A^{1c}_1 v_1\varepsilon_1, \qquad \text{.....(3.9)}$$

where

$$\left.\begin{aligned} A^c_{1111}&=-3k, & A^{oc}_{11}&=-1, \\ A^{1c}_1&=-k, & \lambda_c&=k. \end{aligned}\right\}$$

Since $A^c_{1111}<0$, Eq. (3.9) predicts the unstable symmetric bifurcation buckling corresponding to Thom's typical dual cusp catastrophe.

Then, in such a case, the load-carrying capacity λ_m of the model can be identified as the bifurcation set corresponding to the imperfection sensitivity surface. The surface can be expressed by the following non-dimensionalized form:

$$\tilde{\lambda}_m=\frac{\lambda_m}{\lambda_c}=1\pm\frac{1}{2A^{oc}_{11}\lambda_c}(A^c_{1111})^{1/3}(3A^{1c}_1\varepsilon_1)^{2/3} \qquad \text{.....(3.10)}$$

near the critical point $(v_1, \lambda, \varepsilon_1)=(0, k, 0)$. This sensitivity is usually referred to as the two-thirds power law.

(iii) when $k=\pi^2$

The bifurcations of (i) and (ii) may occur simultaneously. Near the two-fold critical point $(v_1, v_2, \lambda, \varepsilon_1, \varepsilon_2)=(0, 0, k, 0, 0)$, the non-dimensionalized total potential energy of the model can be expanded to the following form:

$$\begin{aligned}A(v_1, v_2, \lambda, \varepsilon_1, \varepsilon_2)=&\frac{1}{24}A^c_{1111}v_1^4+\frac{1}{24}A^c_{2222}v_2^4\\&+\frac{1}{2}(A^{oc}_{11}v_1^2+A^{oc}_{22}v_2^2)(\lambda-\lambda_c)\\&+A^{1c}_1v_1\varepsilon_1+A^{2c}_2v_2\varepsilon_2,\end{aligned} \qquad \text{.....(3.11)}$$

where

$$\begin{aligned}&A^c_{1111}=-3\pi^2, \quad A^c_{2222}=\frac{3}{8}\pi^6, \quad A^c_{1122}=0,\\&A^{oc}_{11}=-1, \quad A^{oc}_{22}=-\frac{1}{2}\pi^2, \quad A^{1c}_1=-\pi^2,\\&A^{2c}_2=-\frac{1}{2}\pi^4, \quad \lambda_c=\pi^2.\end{aligned}$$

Eq. (3.11) predicts the compound bifurcation buckling of the stable symmetric and the unstable symmetric bucklings corresponding to a double cusp catastrophe not included in Thom's seven elementary catastrophes. This catastrophe will not be discussed any further.

(4) Asymmetric Buckling Model

The third model is a column similar to the unstable symmetric buckling model, but having an asymmetric elastic foundation at the right end as shown in Fig. 3.3. Then, the non-dimensionalized total potential energy of the model can be obtained as

$$\begin{aligned}V(w, \lambda, w_0)=&\frac{1}{2}\int_0^1(w,_{xx}^2+w,_{xx}^2w,_x^2)\,dx\\&-\lambda\int_0^1\left(\frac{1}{2}w,_x^2+w,_xw_0,_x+\frac{1}{8}w,_x^4\right)dx\end{aligned} \qquad \text{.....(3.12)}$$

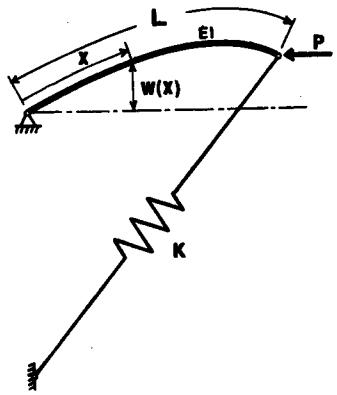

Fig. 3.3. Asymmetric buckling model.

$$+\frac{k}{4}w_L^2+\frac{k}{8}w_L^3-\frac{k}{64}w_L^4+\frac{k}{4}\delta^2-\frac{k}{2}w_L\delta+\frac{k}{8}w_L^2\delta,$$

where

$$\delta\equiv\int_0^1\left(\frac{1}{2}w_{,x}^2+w_{,x}w_{0,x}+\frac{1}{8}w_{,x}^4\right)dx.$$

Let us consider the modal transform $(h_1\times h_2)$:

$$h_1:\ w(x)=v_1x+v_2\sin\pi x$$
$$h_2:\ w_0(x)=\varepsilon_1x+\varepsilon_2\sin\pi x. \qquad \text{.....(3.13)}$$

Upon substitution of Eq. (3.13) into Eq. (3.12), the potential energy, V, can be rewritten as D:

$$D(v_1, v_2, \lambda, \varepsilon_1, \varepsilon_2)=\frac{1}{8}\left(\frac{3}{8}k-\lambda\right)v_1^4+\frac{\pi^2}{4}\left(\pi^2-\lambda+\frac{3}{8}k\right)v_1^2v_2^2$$
$$+\frac{\pi^4}{16}\left(\pi^2-\frac{3}{4}\lambda+\frac{k}{4}\right)v_2^4-\frac{k}{8}v_1^3-\frac{\pi^2}{8}kv_1v_2^2$$
$$+\frac{\pi^2}{4}(\pi^2-\lambda)v_2^2-\lambda v_1\varepsilon_1-\frac{\pi^2}{2}\lambda v_2\varepsilon_2. \qquad \text{.....(3.14)}$$

The following three typical instability phenomena can be shown to take place depending upon the magnitude of the spring constant k:

(i) when $k>2\pi^2$

A distinct bifurcation with mode 2:

$$w(x)=v_2\sin\pi x$$

may occur at the critical point $(v_2, \lambda, \varepsilon_2)=(0, \pi^2, 0)$. Taking into account the interaction term $v_1v_2^2$, the non-dimensionalized total potential energy of the imperfect

model near the critical point can be expanded to the form of

$$A(v_2, \lambda, \varepsilon_2)=\frac{1}{24}A^c_{2222}v_2^4 \qquad \text{.....(3.15)}$$
$$+\frac{1}{2}A^{oc}_{22}(\lambda-\lambda_c)v_2+A^{2c}_2 v_2\varepsilon_2,$$

where

$$A^c_{2222}=D^c_{2222}-3(D^c_{122})^2/D^c_{11}=\frac{-3\pi^4(2\pi^4+\pi^2 k)}{16\left(\frac{k}{2}-\pi^2\right)}<0,$$
$$A^{oc}_{22}=D^{oc}_{22}=-\frac{\pi^2}{2},\quad A^{2c}_2=D^{2c}_2=-\frac{\pi^4}{2},\quad \lambda_c=\pi^2.$$

Since $A^c_{2222}<0$, Eq. (3.15) predicts the unstable symmetric bifurcation buckling corresponding to Thom's dual cusp catastrophe. Then, the bifurcation set near the critical point is in a form similar to Eq. (3.10), and is given by

$$\bar{\lambda}_m=\frac{\lambda_m}{\lambda_c}=1\pm\frac{1}{2A^{oc}_{22}\lambda_c}(A^c_{2222})^{1/3}(3A^{2c}_2\varepsilon_2)^{2/3} \qquad \text{.....(3.16)}$$

(ii) $k<2\pi^2$

A distinct bifurcation with mode 1:

$$w(x)=v_1 x$$

may occur at the critical point $(v_1, \lambda, \varepsilon_1)=(0, k/2, 0)$. The non-dimensionalized total potential energy of the imperfect model near the critical point can be expanded to the form of

$$A(v_1, \lambda, \varepsilon_1)=\frac{1}{6}A^c_{111}v_1^3 \qquad \text{.....(3.17)}$$
$$+\frac{1}{2}A^{oc}_{11}(\lambda-\lambda_c)v_1^2+A^{1c}_1 v_1\varepsilon_1,$$

where

$$A^c_{111}=D^c_{111}=-\frac{3}{4}k,\quad A^{oc}_{11}=-1,\quad A^{1c}_1=-\frac{k}{2},\quad \lambda_c=\frac{k}{2}.$$

Since $A^c_{111}\neq 0$, Eq. (3.17) predicts the asymmetric bifurcation buckling corresponding to Thom's typical fold catastrophe.

The bifurcation set is referred to as the one-half power law, and can be expressed as

$$\bar{\lambda}_m=\frac{\lambda_m}{\lambda_c}=1\pm\frac{1}{A^{oc}_{11}\lambda_c}(2A^c_{111}A^{1c}_1\varepsilon_1)^{1/2}. \qquad \text{.....(3.18)}$$

where, since $A^{oc}_{11}<0$ and $A^{1c}_1<0$ in general, Eq. (3.18) is valid only if $\varepsilon_1<0$ for $A^c_{111}<0$.

(iii) when $k=2\pi^2$

The bifurcations of (i) and (ii) may occur simultaneously. Near this critical point $(v_1, v_2, \lambda, \varepsilon_1, \varepsilon_2)=(0, 0, k/2, 0, 0)$, the total potential energy of the imperfect model can be expanded to the form of

$$\left.\begin{aligned} A(v_1, v_2, \lambda, \varepsilon_1, \varepsilon_2)=&\frac{1}{6}A^c_{111}v_1^3+\frac{1}{2}A^c_{122}v_1v_2^2 \\ &+\frac{1}{2}(A^{oc}_{11}v_1^2+A^{oc}_{22}v_2^2)\,(\lambda-\lambda_c) \\ &+A^{1c}_1v_1\varepsilon_1+A^{2c}_2v_2\varepsilon_2 \end{aligned}\right\} \quad \text{.....(3.19)}$$

where

$$\left.\begin{aligned} &A^c_{111}=D^c_{111}=-\frac{3}{2}\pi^2, \quad A^c_{122}=D^c_{122}=-\frac{\pi^4}{2}, \\ &A^{oc}_{11}=D^{oc}_{11}=-1, \quad A^{oc}_{22}=D^{oc}_{22}=-\frac{\pi^2}{2}, \quad A^{1c}_1=D^{1c}_1=-\pi^2, \\ &A^{2c}_2=D^{2c}_2=-\frac{\pi^4}{2}, \qquad \lambda_c=\pi^2. \end{aligned}\right\}$$

Since

$$A^c_{111}\cdot A^c_{122}=\frac{3}{4}\pi^6<0, \qquad 2\frac{A^{oc}_{11}}{A^{oc}_{22}}-\frac{A^c_{111}}{A^c_{122}}=\frac{1}{\pi^2}>0,$$

Eq. (3.19) predicts the semi-symmetric bifurcation buckling, that is, the homeoclinal bifurcation buckling corresponding to Thom's hyperbolic umbilic catastrophe.

Detailed discussions on the bifurcation sets for each model just mentioned will be described in section 5.

4. Discrete Analysis

(1) General Remarks

A catastrophe analysis through discretization will be presented herein. The discretization adopted herein are the finite element method (abbreviated as FEM) using the ACM shape function, that is, the cubic shape function, and a simplified element method (SEM), idealizing the column to consist of chains of rigid bars and a flexural spring, first introduced by Yamada and Watanabe.[13] These discrete numerical analyses are compared with the continuous analyses. All of the assumptions made for the continuous analysis are also adopted herein. Also, the D. O. F. at each nodal point is two for FEM and one for SEM, respectively. Thus, the total D. O. F. in the SEM is much less than that in the FEM.

The discretized total potential energy corresponding to Eq. (3.3) can be expressed as

$$V(w_i,\ \lambda,\ w_{0j})=\frac{1}{2}K^{B1}_{ij}w_iw_j+\frac{1}{2}K^{B2}_{ijkl}w_iw_jw_kw_l$$
$$-\frac{\lambda}{2}K^{G1}_{ij}w_iw_j-\frac{\lambda}{8}K^{G2}_{ijkl}w_iw_jw_kw_l$$
$$-\lambda K^{G1}_{ij}w_iw_{0j} \qquad \text{.....(4.1)}$$

In Eq. (4.1), K^{B1}_{ij} and K^{B2}_{ijkl} refer to the linear and non-linear flexural stiffness matrices, respectively, whereas, K^{G1}_{ij} and K^{G2}_{ijkl} refer to the linear and non-linear geometrical matrices, respectively. Each subscript i, j, k, l obeys the summation convention up to the total D. O. F., N.

(2) Stable Symmetric Buckling Model

For the perfect model $w_{0j}=0$ ($j=1, 2, \ldots, N$), the characteristic equation at the critical point:

$$\det\ (K^{B1}_{ij}-\lambda K^{G1}_{ij})=0 \qquad \text{.....(4.2)}$$

provides n eigenvector matrices, ϕ_{ij} ($i=1, \ldots, N$; $j=1, \ldots, n$) where n eigenvectors are chosen corresponding to the smallest n eigenvalues.

Then, the following modal transform is applied:

$$w_i=\phi_{ij}v_j \qquad \left\{\begin{matrix} i=1, 2, \ldots, N \\ j=1, 2, \ldots, n \\ 1\leqq n\ll N \end{matrix}\right\} \qquad \text{.....(4.3)}$$

This transform diagonalizes the Hessian matrix of the total potential energy in Eq. (4.1) at the critical point. Upon substitution of Eq. (4.3) into Eq. (4.1), the diagonalized potential energy, D, can be obtained as

$$D(v_i,\ \lambda,\ \varepsilon_j)=\frac{1}{2}\tilde{K}^{B1}_{ij}v_iv_j+\frac{1}{2}\tilde{K}^{B2}_{ijkl}v_iv_jv_kv_l$$
$$-\frac{\lambda}{2}\tilde{K}^{G1}_{ij}v_iv_j-\frac{\lambda}{8}\tilde{K}^{G2}_{ijkl}v_iv_jv_kv_l$$
$$-\lambda\tilde{K}^{G1}_{ij}v_i\varepsilon_j \qquad \text{.....(4.4)}$$

Furthermore, let the same transform, Eq. (4.3), be adopted for the initial deflection w_{0i} ($i=1, 2, \ldots, N$), that is,

$$w_{0i}=\phi_{ij}\varepsilon_j \qquad \left\{\begin{matrix} i=1, 2, \ldots, N \\ j=1, 2, \ldots, n \\ 1\leqq n\ll N \end{matrix}\right\} \qquad \text{.....(4.5)}$$

where ε_j corresponds to v_j($j=1, 2, \ldots, n$), and

$$\left.\begin{aligned} &\tilde{K}^{B1}_{ij}=K^{B1}_{mn}\phi_{mi}\phi_{nj}, \qquad \tilde{K}^{G1}_{ij}=K^{G1}_{mn}\phi_{mi}\phi_{nj}, \\ &\tilde{K}^{B2}_{ijkl}=K^{B2}_{mppq}\phi_{mi}\phi_{nj}\phi_{pk}\phi_{ql}, \\ &\tilde{K}^{G2}_{ijkl}=K^{G2}_{mnpq}\phi_{mi}\phi_{nj}\phi_{pk}\phi_{ql}. \end{aligned}\right\} \qquad \text{.....(4.6)}$$

Table 4.1. Stable symmetric buckling model. —*Cusp Catastrophe*—

	Continuous method	Discretization methods										
		1-D.O.F.	Finite Element Method					Simplified Element Method				
Elements		2	4	8	16	32	64	4	8	16	32	64
D.O.F.		1	8 (3, 5)	16 (7, 9)	32 (15, 17)	64 (31, 32)	128 (63, 65)	3	7	15	31	63
λ_c	9.870	8.000	9.875	9.870	9.870	9.870	9.870	9.373	9.743	9.838	9.862	9.868
A_1^{1c}	−48.705	−32.000	−48.684	−48.699	−48.708	−48.708	−48.708	−43.922	−47.468	−48.393	−48.630	−48.689
A_{11}^{or}	−4.935	−4.000	−4.930	−4.934	−4.935	−4.935	−4.935	−4.686	−4.872	−4.919	−4.931	−4.934
A_{1111}^{c}	360.521 (1.000)	128.000 (0.355)	360.118 (0.999)	360.986 (1.001)	362.534 (1.006)	368.596 (1.022)	392.834 (1.090)	127.889 (0.355)	294.062 (0.816)	343.340 (0.952)	356.190 (0.988)	359.436 (0.997)

Table 4.1 shows the numerical results by the discrete analyses of the model, with those through the continuous analysis and one degree-of-freedom analysis. The convergence of the buckling loads λ_c and the 4th derivatives A^c_{1111} with respect to the number of discrete elements is illustrated in Fig. 4.1. It may be seen that the discretization method can surely realize the instability phenomena of the continuous model.

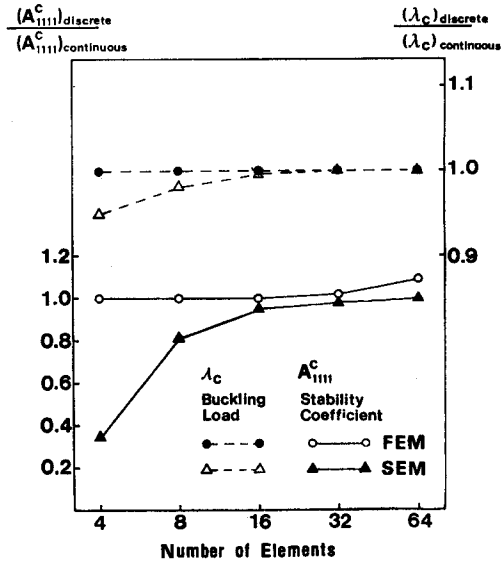

Fig. 4.1. Convergence of buckling load and stability coefficient.

(3) Unstable Symmetric Buckling Model

The discretized total potential energy corresponding to Eq. (3.8) is given by

$$V(w_i, \lambda, w_{0j})=\frac{1}{2}(K^{B1}_{ij}+K^{S}_{ij})w_iw_j+\frac{1}{2}K^{B2}_{ijkl}w_iw_jw_kw_l$$
$$-\frac{\lambda}{2}K^{G1}_{ij}w_iw_j-\frac{\lambda}{8}K^{G2}_{ijkl}w_iw_jw_kw_l$$
$$-\lambda K^{G1}_{ij}w_iw_{0j} \qquad \text{.....(4.7)}$$

where $K^S_{ji}=k\delta_{is}\delta_{js}$, superscript s refers to the spring stiffness, whereas subscript s refers to the nodal point on the elastic foundation, and δ_{ij} designates Kronecker's delta.

For simplicity, a new stiffness parameter κ will be introduced:

$$\kappa\equiv\frac{\pi^2EI}{KL^3}=\frac{\pi^2}{k}, \qquad k=\frac{KL^3}{EI} \qquad \text{.....(4.8)}$$

instead of the non-dimensionalized spring stiffness, k.

Similarly to the continuous analysis, the following typical three instability phenomena may be found to occur, depending on the magnitude of κ:

$0 < \kappa < 1$: stable symmetric bifurcation (cusp catastrophe)

$\kappa = 1$: double cusp catastrophe

$\kappa > 1$: unstable symmetric bifurcation (dual cusp catastrophe)

Table 4.2 shows the numerical results with those of the two-degree-of-freedom analysis and the continuous analysis. As an example, the bifurcation set for $\kappa>1$ in the continuous analysis is illustrated in Fig. 4.2.

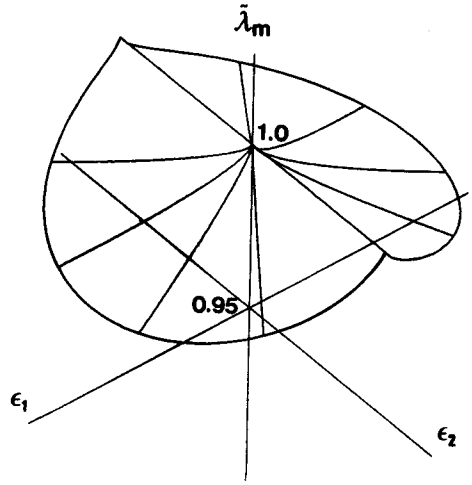

Fig. 4.2. Bifurcation set for unstable buckling model.
— *Dual Cusp Catastrophe* —: $\kappa=1.5$.

(4) Asymmetric Buckling Model

The discretized total potential energy corresponding to Eq. (3.16) is given by

$$
\begin{aligned}
V(w_i, \lambda, w_{0j}) = {} & \frac{1}{2}(K_{ij}^{B1}+K_{ij}^{S4})w_iw_j-\frac{\lambda}{2}K_{ij}^{G1}w_iw_j-\lambda K_{ij}^{G1}w_iw_{0j} \\
& +\frac{1}{2}(K_{ijk}^{S2}+K_{ijk}^{S5})w_iw_jw_k-\frac{\lambda}{8}K_{ijkl}^{G2}w_iw_jw_kw_l \\
& +\frac{1}{2}(K_{ijkl}^{B2}+K_{ijkl}^{S1}+K_{ijkl}^{S3}+K_{ijkl}^{S6})w_iw_jw_kw_l
\end{aligned}
\qquad \text{.....(4.9)}
$$

where

$$
K_{ijkl}^{S1}=\frac{1}{8}kK_{ij}^{G1}K_{kl}^{G1}, \qquad K_{ijk}^{S2}=-\frac{1}{2}k\delta_{ts}K_{jk}^{G1},
$$

$$
K_{ijkl}^{S3}=\frac{1}{8}k\delta_{ts}\delta_{js}K_{kl}^{G1}, \qquad K_{ij}^{S4}=\frac{1}{2}k\delta_{ts}\delta_{js}
$$

$$
K_{ijk}^{S5}=\frac{1}{4}k\delta_{ts}\delta_{js}\delta_{ks}, \qquad K_{ijkl}^{S6}=-\frac{1}{32}k\delta_{ts}\delta_{js}\delta_{ks}\delta_{ts},
$$

Table 4.2(a). Unstable symmetric buckling model. —*Cusp Catastrophe*—

$\kappa \equiv \pi^2 EI/(KL^3)=0.5$

	Continuous method	Discretization methods										
		2-D.O.F.	Finite Element Method					Simplified Element Method				
Elements		2	4	8	16	32	64	4	8	16	32	64
D.O.F.		2	9 (4, 5)	17 (8, 9)	33 (16, 17)	65 (32, 33)	129 (64, 65)	4	8	16	32	64
λ_c	9.870	8.000	9.870	9.870	9.870	9.870	9.870	9.373	9.743	9.838	9.862	9.868
Mode	2	2	2	2	2	2	2	2	2	2	2	2
A_2^{2c}	−48.705	−32.000	−48.684	−48.699	−48.708	−48.708	−48.708	−43.922	−47.468	−48.393	−48.630	−48.689
A_{22}^{oc}	−4.935	−4.000	−4.930	−4.934	−4.935	−4.935	−4.935	−4.686	−4.872	−4.919	−4.931	−4.934
A_{222}^{c}	360.521 (1.000)	128.000 (0.355)	360.118 (0.999)	360.987 (1.001)	362.534 (1.006)	368.596 (1.022)	392.834 (1.090)	127.889 (0.355)	294.062 (0.816)	343.340 (0.952)	356.190 (0.988)	359.436 (0.997)

Table 4.2(b). Unstable symmetric buckling model. —*Double Cusp Catastrophe*—

$\kappa \equiv \pi^2 EI/(kL^3) = 1.0$

	Continuous method	Discretization methods										
		2-D.O.F.	Finite Element Method					Simplified Element Method				
Elements		2	4	8	16	32	64	4	8	16	32	64
D.O.F.		2	9 (4, 5)	17 (8, 9)	33 (16, 17)	65 (32, 33)	129 (64, 65)	4	8	16	32	64
λ_{c1}	9.870	8.000	9.870	9.870	9.870	9.870	9.870	9.870	9.870	9.870	9.870	9.870
λ_{c2}	9.870	8.000	9.875	9.870	9.870	9.870	9.870	9.373	9.743	9.838	9.862	9.868
Mode	1, 2	1, 2	1, 2	1, 2	1, 2	1, 2	1, 2	1, 2	1, 2	1, 2	1, 2	1, 2
A_1^{1c}	−9.870	−8.000	−9.870	−9.870	−9.870	−9.870	−9.870	−9.870	−9.870	−9.870	−9.870	−9.870
A_2^{2c}	−48.705	−32.000	−48.684	−48.699	−48.708	−48.708	−48.708	−43.922	−47.468	−48.393	−48.630	−48.689
A_{11}^{oc}	−1.000	−1.000	−1.000	−1.000	−1.000	−1.000	−1.000	−1.000	−1.000	−1.000	−1.000	−1.000
A_{22}^{oc}	−4.935	−4.000	−4.930	−4.934	−4.935	−4.935	−4.935	−4.686	−4.872	−4.919	−4.931	−4.934
A_{1111}^{c}	−29.609 (1.000)	−29.610 (1.000)	−29.605 (1.000)	−29.595 (1.000)	−29.553 (0.999)	−29.388 (0.993)	−28.724 (0.970)	−28.118 (0.950)	−29.230 (0.987)	−29.514 (0.997)	−29.585 (0.999)	−29.603 (1.000)
A_{2222}^{c}	360.521 (1.000)	128.000 (0.355)	360.671 (1.000)	361.022 (1.001)	362.535 (1.006)	368.596 (1.022)	392.784 (1.090)	127.889 (0.355)	294.062 (0.816)	343.340 (0.952)	356.190 (0.988)	359.437 (0.997)

Table 4.2(c). Unstable symmetric buckling model. —*Dual Cusp Catastrophe*—

$\kappa \equiv \pi^2 EI/(KL^3) = 1.5$

	Continuous method	Discretization methods										
		2-D.O.F.	Finite Element Method					Simplified Element Method				
Elements		2	4	8	16	32	64	4	8	16	32	64
D.O.F.		2	9 (4, 5)	17 (8, 9)	33 (16, 17)	65 (32, 33)	129 (64, 65)	4	8	16	32	64
λ_c	6.580	6.580	6.580	6.580	6.580	6.580	6.580	6.580	6.580	6.580	6.580	6.580
Mode	1	1	1	1	1	1	1	1	1	1	1	1
A_1^{1c}	−6.580	−6.580	−6.580	−6.580	−6.580	−6.580	−6.580	−6.580	−6.580	−6.580	−6.580	−6.580
A_{11}^{oc}	−1.000	−1.000	−1.000	−1.000	−1.000	−1.000	−1.000	−1.000	−1.000	−1.000	−1.000	−1.000
A_{1111}^{c}	−19.739 (1.000)	−19.740 (1.000)	−19.736 (1.000)	−19.725 (0.999)	−19.684 (0.997)	−19.518 (0.989)	−18.854 (0.955)	−19.739 (1.000)	−19.739 (1.000)	−19.739 (1.000)	−19.739 (1.000)	−19.739 (1.000)

and subscript s corresponds to the nodal point on the elastic foundation.

Then, the following typical three instability phenomena may be found to occur, depending on the magnitude of κ introduced in eq. (4.8):

$0 < \kappa < 0.5$: unstable symmetric bifurcation
(dual cusp catastrophe)

$\kappa = 0.5$: homeoclinal bifurcation
(hyperbolic umbilic catastrophe)

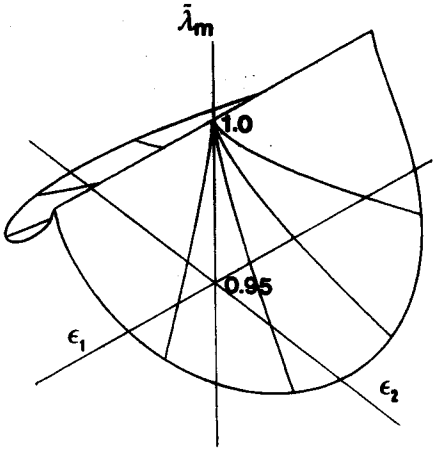

Fig. 4.3. Bifurcation set for asymmetric buckling model.
— *Dual Cusp Catastrophe* —: $\kappa = 0.25$.

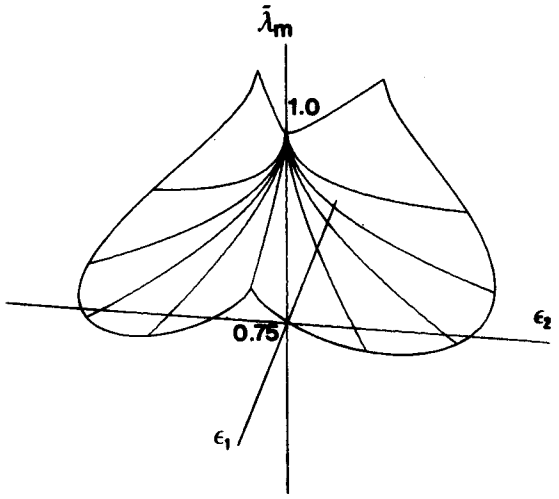

Fig. 4.4(a). Bifurcation set for asymmetric buckling model.
— *Hyperbolic Umbilic Catastrophe* —: $\kappa = 0.5$.
Only the Lowest Sheet of Bifurcation Set is shown.

$\kappa > 0.5$: asymmetric bifurcation
(fold catastrophe)

Table 4.3 shows the numerical results with those of the two-degree-of-freedom analysis and the continuous analysis. The bifurcation sets in the continuous analysis are illustrated in Figs. 4.3, 4.4 and 4.5 for $\kappa=0.25$, 0.5 and 0.75, respectively.

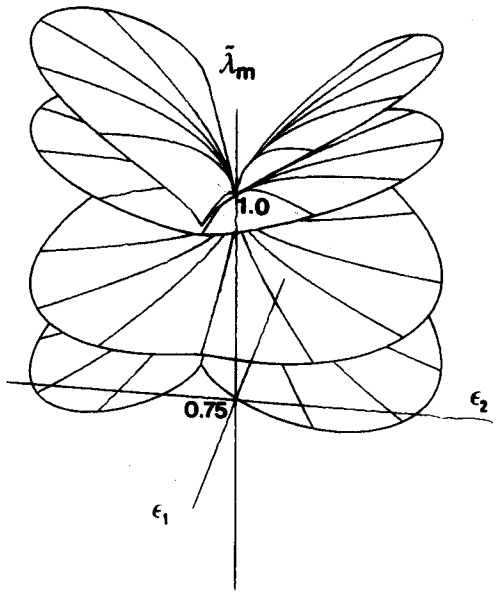

Fig. 4.4(b). Bifurcation set for asymmetric buckling model.
— *Hyperbolic Umbilic Catastrophe* —: $\kappa=0.5$.
All Sheets of Bifurcation Set are shown.

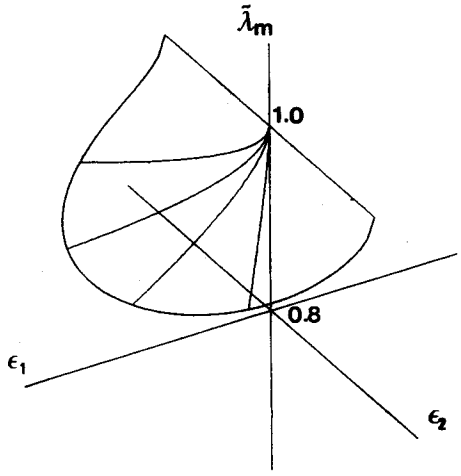

Fig. 4.5. Bifurcation set for asymmetric buckling model.
— *Fold Catastrophe* —: $\kappa=0.75$.

Table 4.3(a) Asymmetric buckling model. —*Dual Cusp Catastrophe*—

$\kappa \equiv \pi^2 EI/(KL^3) = 0.25$

	Continuous method	Discretization methods										
		2-D.O.F.	Finite Element Method					Simplified Element Method				
Elements		2	4	8	16	32	64	4	8	16	32	64
D.O.F.		2	9 (4, 5)	17 (8, 9)	33 (16, 17)	65 (32, 33)	129 (64, 65)	4	8	16	32	64
λ_c	9.870	8.000	9.875	9.870	9.870	9.870	9.870	9.373	9.743	9.838	9.862	9.868
Mode	2	2	2	2	2	2	2	2	2	2	2	2
A_2^{2c}	−48.705	−32.000	−48.684	−48.699	−48.708	−48.708	−48.708	−43.922	−47.468	−48.393	−48.630	−48.689
A_{22}^{oc}	−4.935	−4.000	−4.930	−4.934	−4.935	−4.935	−4.935	−4.686	−4.872	−4.919	−4.931	−4.934
D_{22}^{c}	9.870	11.739	9.865	9.870	9.870	9.870	9.870	10.367	9.996	9.901	9.878	9.872
D_{122}^{c}	−97.409	−78.957	−97.307	−97.403	−97.409	−97.409	−97.409	−92.504	−96.164	−97.096	−97.331	−97.390
D_{2222}^{c}	1802.605	1075.480	1799.186	1802.880	1804.604	1810.678	1834.916	1428.387	1699.504	1776.166	1795.938	1800.941
A_{2222}^{c}	−1081.563 (1.000)	−517.724 (0.479)	−1080.282 (0.999)	−1080.811 (0.999)	−1079.442 (0.998)	−1073.442 (0.992)	−1049.131 (0.970)	−1047.833 (0.969)	−1075.861 (0.994)	−1080.404 (0.999)	−1081.160 (1.000)	−1081.397 (1.000)

Table 4.3(b). Asymmetric buckling model. —*Hyperbolic Umbilic Catastrophe*—

$\kappa \equiv \pi^2 EI/(KL^3) = 0.5$

	Continuous method	Discretization methods										
		2-D.O.F.	Finite Element Method					Simplified Element Method				
Elements		2	4	8	16	32	64	4	8	16	32	64
D.O.F.		2	9 (4, 5)	17 (8, 9)	33 (16, 17)	65 (32, 33)	129 (64, 65)	4	8	16	32	64
λ_{c1}	9.870	8.000	9.870	9.870	9.870	9.870	9.870	9.870	9.870	9.870	9.870	9.870
λ_{2c}	9.870	8.000	9.875	9.870	9.870	9.870	9.870	9.373	9.743	9.838	9.862	9.868
Mode	1, 2	1, 2	1, 2	1, 2	1, 2	1, 2	1, 2	1, 2	1, 2	1, 2	1, 2	1, 2
A_1^{1c}	−9.870	−8.000	−9.870	−9.870	−9.870	−9.870	−9.870	−9.870	−9.870	−9.870	−9.870	−9.870
A_2^{2c}	−48.705	−32.000	−48.684	−48.699	−48.708	−48.708	−48.708	−43.922	−47.468	−48.393	−48.630	−48.689
A_{11}^{oc}	−1.000	−1.000	−1.000	−1.000	−1.000	−1.000	−1.000	−1.000	−1.000	−1.000	−1.000	−1.000
A_{22}^{oc}	−4.935	−4.000	−4.930	−4.934	−4.935	−4.935	−4.935	−4.686	−4.872	−4.919	−4.931	−4.934
A_{111}^{c}	−14.804 (1.000)	−12.000 (0.811)	−14.804 (1.000)	−14.804 (1.000)	−14.804 (1.000)	−14.804 (1.000)	−14.804 (1.000)	−14.804 (1.000)	−14.804 (1.000)	−14.804 (1.000)	−14.804 (1.000)	−14.804 (1.000)
A_{122}^{c}	−48.705 (1.000)	−32.000 (0.657)	−48.654 (0.999)	−48.701 (1.000)	−48.704 (1.000)	−48.705 (1.000)	−48.713 (1.000)	−46.252 (0.950)	−48.082 (0.987)	−48.584 (0.997)	−48.665 (0.999)	−48.695 (1.000)

Table 4.3(c). Asymmetric buckling model. —*Fold Catastrophe*—

$\kappa \equiv \pi^2 EI/(KL^3) = 0.75$

	Continuous method	Discretization methods										
		2-D.O.F.	Finite Element Method					Simplified Element Method				
Elements		2	4	8	16	32	64	4	8	16	32	64
D.O.F.		2	9 (4, 5)	17 (8, 9)	33 (16, 17)	65 (32, 33)	129 (64, 65)	4	8	16	32	64
λ_c	6.580	6.580	6.580	6.580	6.580	6.580	6.580	6.580	6.580	6.580	6.580	6.580
Mode	1	1	1	1	1	1	1	1	1	1	1	1
A_1^{1c}	−6.580	−6.580	−6.580	−6.580	−6.580	−6.580	−6.580	−6.580	−6.580	−6.580	−6.580	−6.580
A_{11}^{oc}	−1.000	−1.000	−1.000	−1.000	−1.000	−1.000	−1.000	−1.000	−1.000	−1.000	−1.000	−1.000
A_{111}^{c}	−9.870 (1.000)	−9.870 (1.000)	−9.870 (1.000)	−9.870 (1.000)	−9.870 (1.000)	−9.870 (1.000)	−9.870 (1.000)	−9.870 (1.000)	−9.870 (1.000)	−9.870 (1.000)	−9.870 (1.000)	−9.870 (1.000)

5. Discussions

Detailed discussions will be presented herein based on Tables 3.1, 4.1, 4.2 and 4.3, and Figs. 4.1, 4.2, 4.3 and 4.4, comparing the numerical results of both the continuous and discrete analyses.

Table 3.1 shows how the degree of the order of the approximation for either a curvature, κ_x, or a shortening, Δ, may affect the form of the total potential energy. The first order approximations in the first row give a linear eigenvalue problem, from which only a critical bifurcation buckling load can be evaluated. The fourth order approximations in the last row are found to describe the geometrical non-linearity with sufficient accuracy. The second and third rows in the table indicate that the potential energies fail to evaluate rigorously either the flexural strain energy or the external work.

Three tables in Section 4 provide a complete comparison among the numerical results of stability coefficients such as A^c_{111}, A^c_{1111}, for the one-degree-of-freedom, two-degree-of-freedom, continuous and discrete analyses, respectively.

Furthermore, in these tables, the two figures in parentheses in the second row, pertaining to the FEM, refer to the D. O. F. of the lateral deflection and that of the rotation, respectively. And, the value in parentheses in the rows of stability coefficients such as A^c_{111}, A^c_{1111}, indicate the ratio of the value of each coefficient through discrete analyses to the value of the corresponding coefficient through the continuous analyses.

Table 4.1 shows the numerical results for the stable symmetric buckling model. Fig. 4.1 illustrates the convergence of the buckling loads and the 4th order stability coefficients A^c_{1111} with respect to the number of finite elements. Obviously, the discrete analyses can be shown to realize the instability phenomena, predicted by the continuous anlysis. The FEM used herein, however, may seem to tend to estimate the values of A^c_{1111} slightly larger than the SEM, with an increase of the number of elements.

The numerical results are shown in Table 4.2 for the unstable symmetric buckling model. In this case, the discrete analysis can be also shown to realize the continuous model. Similarly, the FEM will tend to overestimate slightly the values of A^c_{1111}, A^c_{2222} etc, in comparison with the SEM.

Fig. 4.2 illustrates a bifurcation set for $\kappa>1$ in the continuous analysis. The surface of the bifurcation set represents the dual cusp catastrophe with respect to the buckling mode 1, i.e, the mode for the buckling of the column structure. It is symmetric with respect to the plane of $\varepsilon_1=0$, or $\varepsilon_2-\lambda$ plane. Furthermore, it has no dependence on the value of ε_2, which is called the two-thirds power law. For

example, if $\varepsilon_1=1/1000$, $\varepsilon_2=0$, then $\tilde{\lambda}_m=0.985$. The load-carrying capacity will thus be reduced by 1.5%, compared to the buckling load.

Table 4.3 shows the numerical results for the asymmetric buckling model. The bifurcation sets in the continuous analysis are illustrated in Figs. 4.3, 4.4 and 4.5 for $\kappa=0.25$, 0.5 and 0.75, respectively.

A bifurcation set for $\kappa=0.25$ is shown in Fig. 4.3. The surface of the bifurcation set corresponds to the dual cusp catastrophe with respect to the buckling mode 2, i.e., the straight line rigid-body mode. It is symmetric with respect to the plane $\varepsilon_2=0$ independent of ε_1. For example, if $\varepsilon_1=0$, $\varepsilon_2=1/1000$, then $\tilde{\lambda}_m=0.971$, so that the load-carrying capacity will be reduced by 2.9%, compared to the buckling load.

Fig. 4.4 illustrates the bifurcation sets of a typical hyperbolic umbilic catastrophe for $\kappa=0.5$. The bifurcation point has been called the homeoclinal bifurcation point of the semi-symmetric buckling by Thompson. For example, if $\varepsilon_1=0$, $\varepsilon_2=1/1000$, then $\tilde{\lambda}_m=0.851$, and if $\varepsilon_1=1/1000$, $\varepsilon_2=0$, then $\tilde{\lambda}_m=0.937$. Thus, the load-carrying capacity will be reduced by 14.9% and 6.4%, respectively, from the buckling load.

Fig. 4.5 illustrates the bifurcation set of a fold catastrophe with respect to the buckling mode 1 for $\kappa=0.75$. It will exist only if $\varepsilon_1>0$ independently on ε_2. For example, if $\varepsilon_1=1/1000$, $\varepsilon_2=0$, then $\tilde{\lambda}_m=0.923$, whereby the load-carrying capacity will be reduced by 7.7% from the buckling load.

From these numerical results, the effects of the initial imperfections on the load-carrying capacity may be found to be significantly sensitive for the asymmetric buckling model. The imperfection sensitivity to mode 2, ε_2 of the compound buckling for $\kappa=0.5$, may seem to be much greater than that of a distinct buckling of mode 2 for $\kappa=0.25$.

Next, several discussions on the error and convergence of each stability coefficient may be made. The values of the stability coefficients calculated by a discrete analysis may converge to those in a continuous analysis, as the number of discretized elements increases. Especially, the stability coefficients through the SEM may converge rapidly to the value through the continuous analysis. The value by the FEM, on the other hand, may have a tendency to overestimate slightly, as the number of elements becomes larger. The FEM provides a very accurate value of the buckling loads regardless of any kinds of models and buckling modes.

The values of the stability coefficients for the rigid buckling mode 1 of the elastic foundation can be evaluated precisely for any modes, and in any analyses. Those for mode 2 of the column structure, however, may contain slight errors depending on the degree of approximation of the mode shape.

6. Conclusions

For several simple elastic conservative column structures, both continuous and discrete analyses were performed. The numerical results were compared with the two-degree-of-freedom analyses.

The following conclusions may be summarized as:

(1) The discrete analysis can be shown to realize the instability phenomena, predicted by the continuous analysis. The results of the discrete analysis are shown to converge to those of the continuous analysis generally, as the number of discrete finite elements increases.

(2) The imperfection sensitivity of structures can be evaluated qualitatively and quantitatively by means of the bifurcation set in the control space through the catastrophe theory.

(3) For a legitimate evaluation of the "cusp and dual cusp catastrophe", the 4th order non-linear terms must be considered rigorously in expressions for both the strain energy and the external work. Then, the stable symmetric buckling model is shown to indicate the typical cusp catastrophe.

(4) The unstable symmetric buckling model can be shown to indicate the typical dual cusp catastrophe for a relatively small stiffness of the elastic foundation, the cusp catastrophe for a relatively large stiffness, and the compound double cusp catastrophe at a certain critical stiffness value.

(5) The asymmetric buckling model can be shown to indicate the typical fold catastrophe for a relatively small stiffness of the inclined elasic foundation, the dual cusp catastrophe for a relatively large stiffness, and the compound hyperbolic umbilic catastrophe at a certain critical stiffness value.

(6) The value of each stability coefficient calculated by the SEM may converge to that by the continuous analyses.

(7) The value of each stability coefficient calculated by the FEM may tend to overestimate slightly in comparison with the SEM, as the number of discrete finite elements increases.

(8) The true load-carrying capacity of the column structure should be investigated, taking into account such things as the extensibility, the elasto-plasticity of material and the residual stresses of the cross section.

This study was financially assisted by a Grant-in-aid for Scientific Research from the Ministry of Education, Science and Culture in the years of 1981 and 1982.

Bibliographies

1) Koiter, W.T.: On the stability of equlibrium (in Dutch with English summary), Theses, Delft, Amsterdam, 1945. English transactions (NASA TT, F10, 833, 1967 and AFFDL-TR-70-25,

1970).
2) Thompson, J.M.T.: A general theory for the equilibrium and stability of discrete conservative systems, J. Appl. Math. Phys. (ZAMP), Vol. 20, 1969, pp. 797–846.
3) Thom, R.: Structural Stability and Morphogenesis, Benjamin, Reading, Massachusetts, 1975.
4) Zeeman, E.C.: Euler buckling, in Structural Stability, the Theory of Catastrophes, and Applications in the Sciences, Lecture Notes in Mathematics, Springer-Verlag, Berlin, Vol. 525, 1976, pp. 373–395.
5) Thompson, J.M.T. and G.W. Hunt: A General Theory of Elastic Stability, Wiley, London, 1973.
6) Thompson, J.M.T. and G.W. Hunt: Towards a unified bifurcation theory, J. Appl. Math. Phys. (ZAMP), Vol. 26, 1975, pp. 581–603.
7) Thompson, J.M.T., J.K.T. Tan, and K.C. Lin: On the topological classification of post-buckling phenomena, J. Struct. Mech., Vol. 6, No. 4, 1978, pp. 384–414.
8) Niwa, Y., E. Watanabe, and N. Nakagawa: Catastrophe and imperfection sensitivity of two-degree-of-freedom systems, Proc. of JSCE, No. 307, March 1981, pp. 99–111.
9) Thompson, J.M.T. and G.W. Hunt: Comparative perturbation studies of the Elastica, Int. J. Mech. Sci., Vol. 11, 1969, pp. 999–1014.
10) Roorda, R.: Stability of structures with small imperfections, J. Engng. Mech. Div., ASCE, Vol. 91, No. EM1, 1965, pp. 87–106.
11) Niwa, Y., E. Watanabe, and H. Isami: Catastrophe analysis of structures by discretization and modal transforms, Memoirs of the Faculty of Engineering, Kyoto University, Vol. 43, Part 1, 1981, pp. 67–87.
12) Poston, T. and I.N. Stewart: Catastrophe Theory and Its Applications, Pitman, 1978.
13) Yamada, Y., E. Watanabe, and R. Ito: Compressive strength of plates with closed-sectional ribs, Proc. of JSCE, No. 278, 1978, pp. 133–147.